JOURNAL OF APPLIED ELECTROCHEMISTRY 19 (1989) 839–843

Mechanism of nickel–molybdenum alloy electrodeposition in citrate electrolytes

E. CHASSAING, K. VU QUANG

Centre d'Etudes de Chimie Métallurgique – CNRS, 15 Rue Georges Urbain, 94407 Vitry-sur-Seine, France

R. WIART

Laboratoire propre no 15 du CNRS, 'Physique des Liquides et Electrochimie', Université P. et M. Curie, 4 pl. Jussieu, 75252 Paris Cedex 05, France

Received 6 December 1988; revised 20 February 1989

The kinetics of the induced codischarge of Mo with Ni in citrate–ammonia electrolytes was investigated by means of polarization and a.c. impedance measurements. Three potential ranges were considered. At low polarization, hydrogen evolution resulting from citrate reduction is the main reaction. The impedance plots exhibit a large capacitive loop with a small high frequency inflection characteristic of the development of a porous layer and a low frequency inductive feature. At intermediate polarization, the partial currents for Ni and Mo discharge increase in the same proportion; the hydrogen evolution is first constant and then rapidly decreases. Then a large low-frequency capacitive feature is observed on the impedance plots, whose size decreases with increasing polarization. At still higher polarization, the Mo discharge becomes increasingly controlled by diffusion which generates an additional capacitive loop. A reaction scheme is proposed which accounts for the polarization data and the major impedance features.

1. Introduction

Owing to the high corrosion resistance of the Ni–Mo alloys containing about 27 wt % Mo, many investigations have been devoted to the electrodeposition of these layers. Ni–Mo alloy coatings were then prepared using direct current or pulse plating [1–4]. However the mechanism of molybdenum electrocrystallization is still not elucidated. Indeed this metal has never been deposited in a pure state from aqueous solutions whereas its codeposition with iron-group metals is possible [5]. Several hypotheses have been proposed. The most recent investigation mentioned the possible multistep reduction of some molybdic species leading to a molybdenum oxide which would be reduced by atomic hydrogen previously adsorbed on the inducing metal [6].

Aiming at a better understanding of the Ni–Mo codeposition kinetics, the present study was carried out using a.c. impedance measurements in addition to steady-state polarization investigations.

2. Experimental procedure

The solutions were made up from analytical grade purity Prolabo or Merck compounds and distilled deionized water. The electrolytes contained nickel sulfate, sodium molybdate and trisodium citrate as a complexing agent (Table 1). The pH was adjusted with ammonia to 9.5 for which the alloy deposition efficiency is high and crack-free deposits can be obtained (2). The temperatures was kept at 37° C. The solutions were deaerated by argon bubbling. The effect of molybdate concentration (electrolytes A, B, C) was investigated. Additional experiments with citrate and molybdate citrate electrolytes, free of nickel, were also carried out.

The cathode was a nickel disc, made of Johnson–Matthey high-purity nickel (less than 10 ppm impurities) of 0.5 cm diameter rotating at up to 2500 rev min^{-1}. Some experiments were also performed using a high purity molybdenum disc (area 0.45 cm^2) to investigate the role of the substrate nature. The anode was a platinum gauze of large surface area.

The potentials are referred to a saturated sulfate electrode (SSE) and are corrected for ohmic drop. The current potential curves corresponding to steady states were recorded potentiostatically at low polarization, and galvanostatically at higher polarization.

A.c. impedance measurements in the range 60 kHz–5 mHz, were carried out using a Solartron 1250 analyser and a 1186 Schlumberger interface monitored by an Apple IIe microcomputer.

For chemical analysis, the layers deposited on platinum or stainless steel substrates were peeled off

Table 1. Electrolyte compositions (mol dm^{-3})

Electrolyte	*A*	*B*	*C*	*D*
Na_2MoO_4, $2H_2O$	0.0075	0.015	0.030	0
$NiSO_4$, $7H_2O$		0.2		
Na_3Cit, $2H_2O$		0.25		

0021-891X/89 $03.00 + .12 © 1989 Chapman and Hall Ltd.

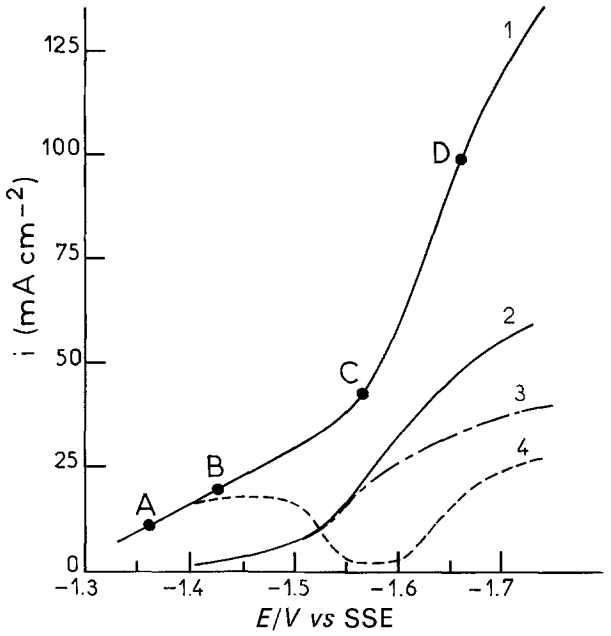

Fig. 1. Steady-state polarization curves for electrolyte B; electrode rotation speed: 1000 rev min^{-1}: (1) global polarization curve; (2) partial curve for nickel discharge; (3) partial curve for molybdenum discharge; (4) partial curve for hydrogen discharge.

and the nickel was analysed after dissolution by complexometry with EDTA [7]. The molybdenum content was deduced by difference. The faradaic efficiencies and the total and partial polarization curves were then derived. Some SEM observations and EDAX analysis of the deposits were also performed.

3. Steady state behaviour

For the considered electrolytes, the polarization curves are shifted towards less negative potentials when the electrode rotation speed is increased, indicating a mass transport effect on the discharge process. When the molybdate and/or the nickel sulphate concentration are increased, the electrode is also depolarized.

The global and partial polarization curves are shown in Fig. 1 for electrolyte B and an electrode rotation speed of 1000 rev min^{-1}.

At low polarizations, i.e. E > −1.4 V vs SSE, the current efficiency of metal deposition is very low. Hydrogen evolution is observed, as in the case of pure citrate or molybdate/citrate solutions.

In the intermediate polarization range, between −1.4 and −1.5 V, the hydrogen discharge partial current is nearly potential independent. The larger the bulk molybdate concentration, the higher this current plateau. For potentials between −1.50 and −1.55 V, the partial current for hydrogen evolution rapidly decreases. In the potential range −1.40 to −1.55 V, the partial currents for nickel and molybdenum increase at the same rate and are approximately equal. The alloy composition remains nearly constant: 35 Mo wt % with electrolyte A, 38 wt % with electrolyte C. This corresponds approximately to the composition of the Ni_3Mo intermetallic phase. However the deposit also contains oxygen and hydrogen [8].

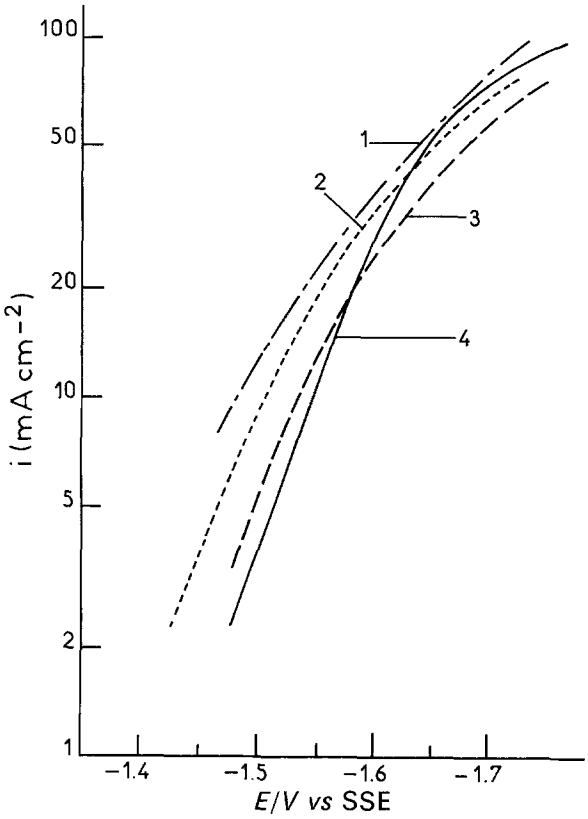

Fig. 2. Steady-state polarization curves for nickel discharge; electrode rotation speed: 1000 rev min^{-1}: (1), (2), (3) and (4) respectively for electrolytes A, B, C and D.

The presence of the Ni_3Mo intermetallic phase could not be identified by X-ray diffraction since the alloys deposited in this potential range were poorly crystallized.

At more negative potentials, the partial current for nickel discharge increases more rapidly than that for molybdenum discharge. The higher the bulk molybdate concentration is, at the more negative potentials this effect occurs (−1.50, −1.55, −1.60 V with electrolytes A, B and C respectively). At still higher polarization (e.g. for E < −1.7 V in Fig. 1), the molybdenum partial current becomes proportional to the square root of the electrode rotation speed. This indicates that the molybdenum discharge is controlled by mass transport of the molybdic species towards the cathode. The hydrogen evolution increases again though the amount of included hydrogen is still decreasing [8].

The nickel deposition rate is affected by the coreduction of the molybdic species (Fig. 2): at low polarization the nickel discharge is enhanced in the alloy electrolytes, as compared to that of separate nickel deposition from citrate solutions (curve 4). At more negative potentials an opposite trend is observed; the larger the molybdate concentration, the more inhibited the nickel deposition.

4. Impedance measurements

At low polarizations, the impedance diagrams exhibit a large capacitive loop with an inflection in the high

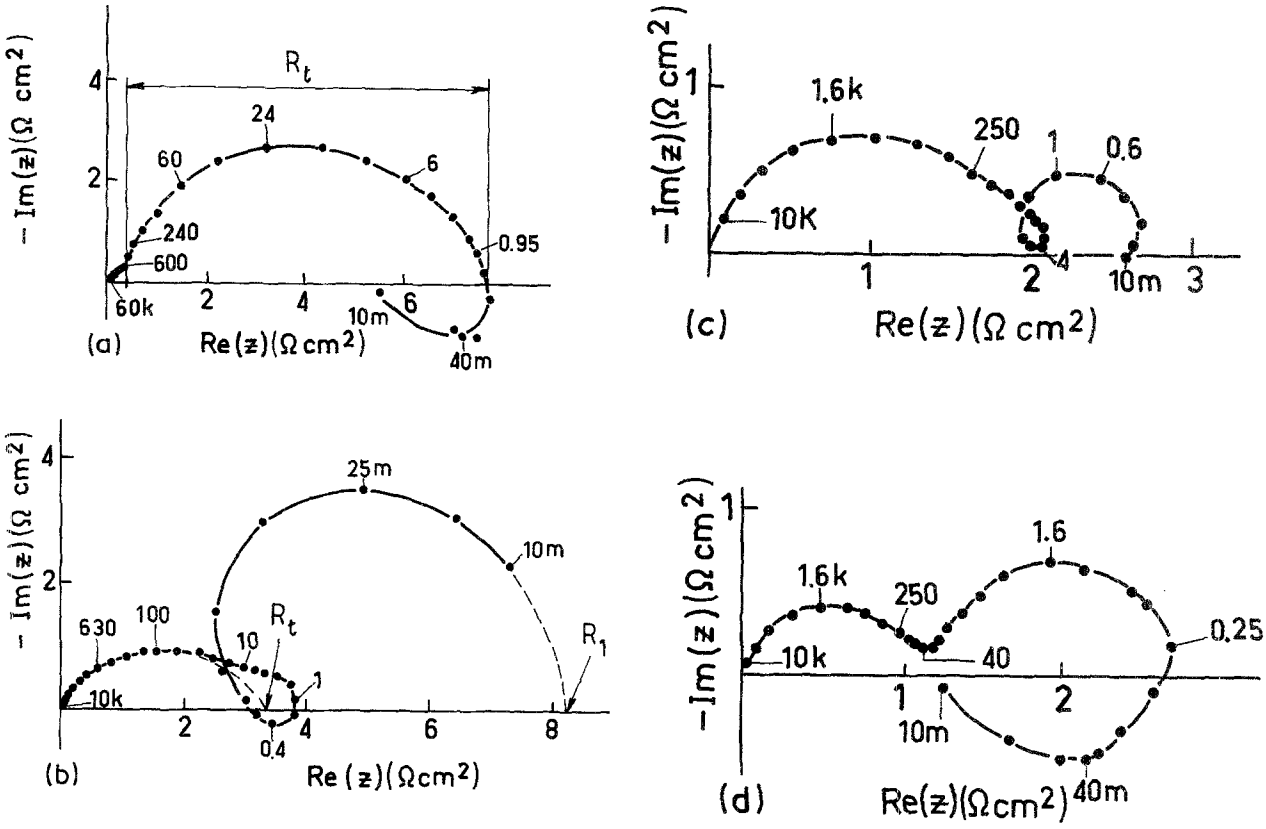

Fig. 3. Impedance plots recorded in electrolyte B at points A, B, C, D in Fig. 1; electrode rotation speed: 1000 rev min^{-1}: (a) i = 11 mA cm^{-2}, E = − 1.365 V/SSE; (b) i = 20 mA cm^{-2}, E = − 1.425 V/SSE; (c) i = 40 mA cm^{-2}, E = − 1.565 V/SSE; (d) i = 100 mA cm^{-2}, E = − 1.680 V/SSE.

frequency range (Fig. 3a). This inflection becomes more pronounced with increasing polarization time before stabilization at the steady state, whatever the substrate nature: nickel, molybdenum or Ni–Mo deposits (prepared at high current densities). Simultaneously the capacitance measured from the apex frequency of the capacitive loop becomes larger: for example at − 1.42 V it increases from 240 μF cm^{-2} at 1 min, to 15 mF cm^{-2} at 95 min polarization. A small inductive feature is observed whose characteristic frequency increases exponentially with polarization independently of the electrode rotation speed (Fig. 4). For electrode polarization lower than − 1.55 V the $R_t i$ product of the current density, i, and the charge transfer resistance, R_t, decreases with increasing polarization or decreasing molybdate concentration (Fig. 5) i.e. when the hydrogen discharge partial current is lowered (see Fig. 1). Because of the distortion of the capacitive loop due to the interference with an additional feature at medium frequencies (Fig. 3b and c), R_t was obtained by extrapolation, which contributes to the scatter of the results.

At intermediate polarizations (− 1.40 to − 1.55 V), in addition to the above-mentioned features, there appears a large capacitive loop corresponding to lower frequencies, ca. 25 mHz (Fig. 3b). As shown in Fig. 3b and c, the relative size of this loop, estimated by the ratio R_l/R_t, (R_l = maximum of the impedance real part) decreases with increasing polarization (Fig. 6). In addition the larger this loop size, the higher the bulk molybdate concentration. This loop is probably associated with the hydrogen evolution reaction, whose current (i) is constant and then rapidly decreases with increasing polarization (see Fig. 1) and (*ii*) increases with the bulk molybdate concentration.

At higher polarizations (E < − 1.6 V), the size of

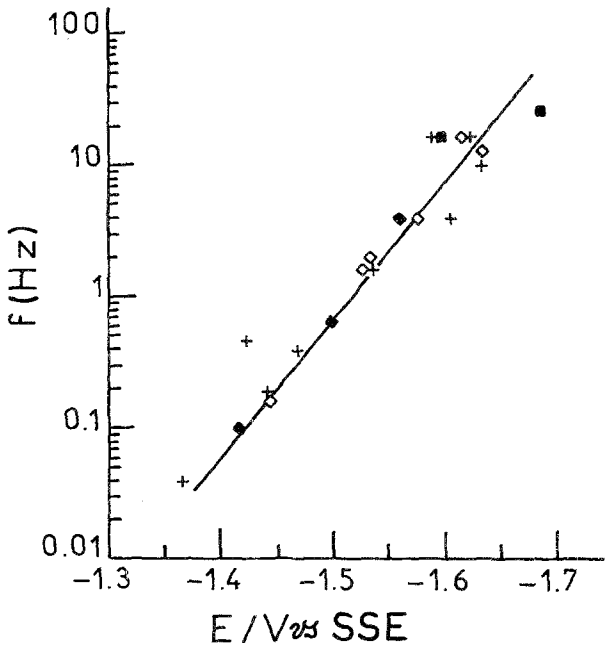

Fig. 4. Potential dependence of the characteristic frequency of the inductive loop at various electrode rotation speeds for electrolyte B. (◆) 2000, (+) 1000, (◇) 500, (■) 250 rev min^{-1}.

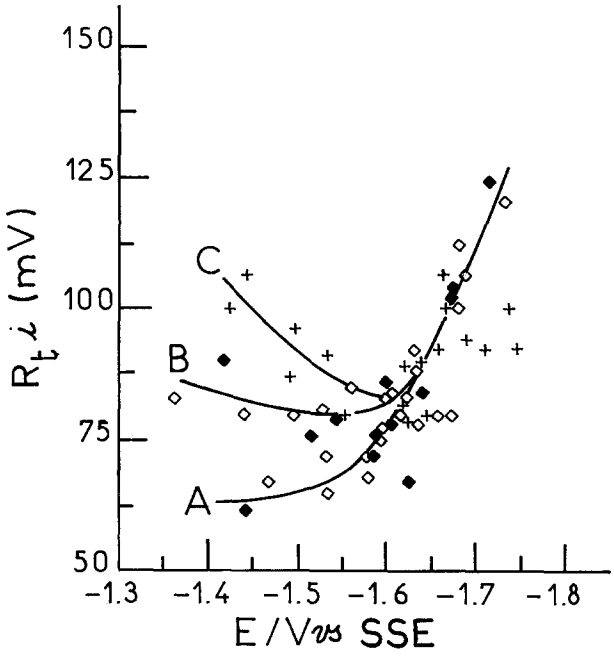

Fig. 5. Potential dependence of the $R_t i$ product of R_t charge transfer resistance and i, current density. Electrolytes A (◆), B (◇), C (+); rotation speed 500–2000 rev min^{-1}.

this additional capacitive loop increases again (Fig. 3d). The characteristic frequency of this capacitive feature becomes potential independent and proportional to the electrode rotation speed (Fig. 7). The minimum of R_1/R_t occurs at the more negative potentials the higher the bulk molybdate concentration is (Fig. 6). As shown in Fig. 5, the $R_t i$ product also increases with increasing polarization; it might then be controlled by the hydrogen discharge current which also increases in this range of polarizations (see Fig. 1).

5. Discussion

Several investigations have been devoted to the induced codeposition mechanism of molybdenum

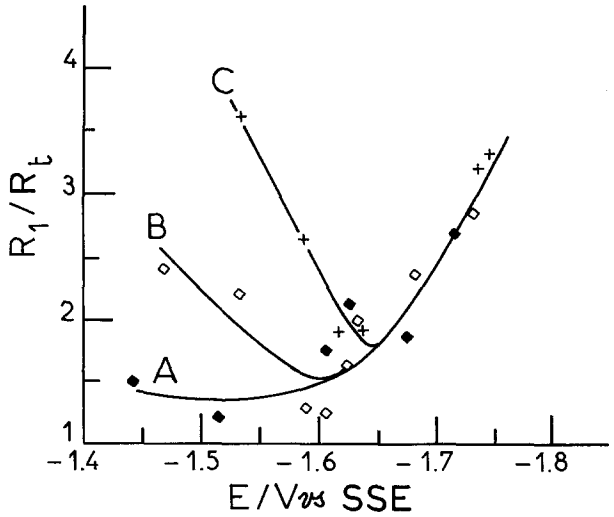

Fig. 6. Potential dependence of the R_1/R_t ratio (R_1 maximum of the impedance real part) for electrolytes A, B and C. Rotation speed 1000 rev min^{-1}.

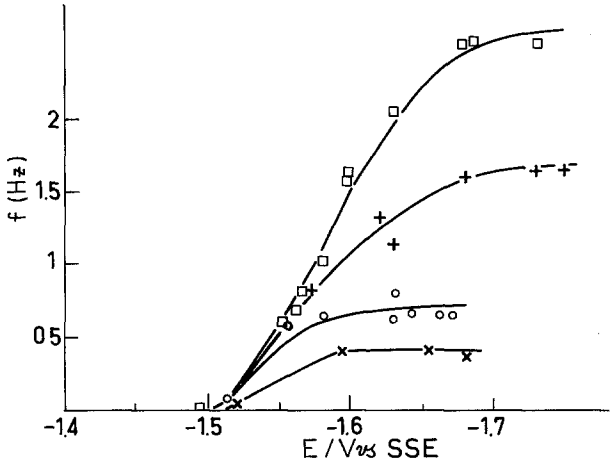

Fig. 7. Potential dependence of the characteristic frequency of the medium frequency capacitive loop at various electrode rotation speeds for electrolyte B. ■, 2000 rev min^{-1}; +, 1000 rev min^{-1}; ○, 500 rev min^{-1}; ×, 250 rev min^{-1}.

with the iron group metals. According to Brenner, who was the first to sum up the various hypotheses up to 1963, there would be a transfer of the polarization energy of the inducing metal (Ni) to the molybdate, allowing the codischarge of molybdenum [5]. More recently, Kroeger showed that interactions between the components in the deposit may considerably shift the deposition potential of the less noble component and enable the induced codeposition [9].

The most valuable contribution stems from Fukushima *et al.* who showed the multi-step reduction of the molybdic species. The partly reduced oxide would be further reduced by atomic hydrogen adsorbed on the inducing metal [6]. However the authors did not verify their reaction scheme by electrochemical investigations.

In order to study the specific contribution of the various species, electrolytes containing only citrate and molybdate/citrate were also investigated. In pure 0.25 M sodium citrate solutions, no reaction occurs in a large polarization range on a nickel substrate; at potentials more negative than −1.6 V, hydrogen evolution is observed. The impedance plots exhibit only a capacitive loop attributed to the charge transfer resistance in parallel with the double layer capacity. The $R_t i$ product is nearly constant and equal to ca. 100 mV; it indicates an irreversible charge transfer exponentially activated with potential. The polarization curve and the impedance plots are not affected by ammonia additions. In the solutions (pH > 8), protons are not likely to reduce. However citrate would probably release the labile hydrogen of the alcohol function according to the reduction reaction:

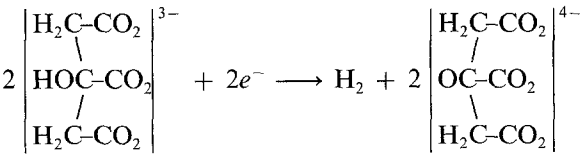

(1)

In molybdate/citrate electrolytes, when a nickel or a molybdenum substrate is polarized at −1.4 V, the

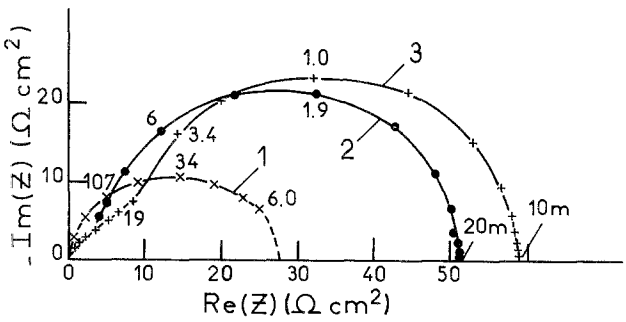

Fig. 8. Time dependence of the impedance diagrams recorded at −1.6 V/SSE, at 1000 rev min^{-1} in 0.03 M Na_2MoO_4,0.025 M Na_3Cit: (1) Δt = 15 sec, i = 4 mA cm^{-2}; (2) Δt = 53 min, i = 2.15 mA cm^{-2}; (3) Δt = 130 min, i = 2.0 mA cm^{-2}.

cathodic current density, slightly higher on Ni than on Mo, continuously decreases with time. After polarization an iridescent layer is observed which might be a molybdenum oxide, possibly MoO_2 involved in Fukushima's model [6]. Indeed this oxide, identified by ESCA analysis, has been shown to form after reduction of molybdate in alkaline solutions [10]. Also thermodynamic data indicate the possible formation of MoO_2 by reduction of molybdate anions at −1.43 V vs SSE [11]:

$$MoO_4^{2-} + 2H_2O + 2e^- \longrightarrow MoO_2 + 4OH^- \quad (2)$$

The impedance data indicate the progressive formation of a porous layer (Fig. 8). The capacitive loop is increasingly more pronounced showing an inflection in the high frequency range; in addition the capacitance value is an increasing function of the polarization time (respectively 160 μF cm^{-2}, 1.7 mF cm^{-2} and 3 mF cm^{-2} after 15 sec, 53 min and 130 min), thus indicating a growing surface area. The $R_t i$ product remains constant and equal to ca. 100 mV, as in the case of pure citrate electrolytes. Consequently it can be concluded that the same reaction (1) for hydrogen evolution proceeds through the oxide layer (electronic conductor) slowly formed according to reaction (2). During the layer formation, the oxide surface area would increase with time but the electrode reactivity for hydrogen evolution, related to the layer conductivity, would decrease.

In Ni–Mo–citrate electrolytes, when a nickel, or molybdenum or Ni–Mo deposit electrode is polarized in the range −1.35 V to −1.45 V, the current density which mainly corresponds to hydrogen evolution increases with time and stabilizes at higher values than in pure citrate or Mo–citrate solutions. However a 6 hr polarization of the electrode at −1.35 V leads to the formation of an iridescent layer. According to preliminary semi-quantitative AES analysis, this 250 Å thick layer probably contains molybdenum oxide and nickel with an approximate Ni/Mo atomic ratio = 80/20, then corresponding to the formula MoO_2Ni_4. Impedance data again indicate the development of a porous layer whose area increases with time as in Mo/citrate solutions. EDAX analysis of the layer formed on an iron substrate confirms the presence of Ni–Mo layers of approximately 80/20 atomic ratio. Fukushima's experiments also confirm the presence of a surface film on the electrode whose resistivity would be the higher the larger the molybdenum content, i.e. at low polarization [6a]. The formation of such a layer of increasing reactivity with polarization might contribute to the inductive feature observed on diagram A in Fig. 1.

It can be concluded that the presence of Ni^{2+} ions allows the transformation of the Mo oxide MoO_2 into a mixed NiMo oxide, written MoO_2Ni_4 to account for AES and EDAX data, according to:

$$MoO_2 + 4Ni^{2+} + 8e^- \rightleftharpoons MoO_2Ni_4 \quad (3)$$

With increasing polarization, the increasing electrode coverage by this oxide, which would help the citrate reduction to take place (reaction 1), can explain the inductive feature whose characteristic frequency increases exponentially with potential as experimentally observed. Such a situation might be consistent with a potential activated increase in the electrode coverage, assuming that reaction (3) is exponentially activated with potential. Indeed it was shown that when an electrode was polarized in the range −1.3 to −1.6 V in electrolyte A and then transferred and polarized at −1.6 V in 0.25 M citrate solution, the current density for hydrogen discharge was higher than for the bare substrate. This confirms that a Ni–Mo alloy deposit is a catalyst for hydrogen evolution [12].

At potentials more negative than −1.4 V, hydrogen evolution does not increase further and decreases rapidly at E < −1.5 V. It can be assumed that the mixed oxide is reduced according to a slow reaction which produces a surface compound acting as an inhibitor for hydrogen evolution, thus generating the low frequency capacitive loop observed experimentally at 25 mHz. This slow inhibition process for hydrogen evolution would be coupled with the relatively fast global reaction (4) leading to the alloy deposit of formula $MoNi_3$ corresponding to experimental alloy analyses:

$$MoO_4^{2-} + 3Ni^{2+} + 8e^- + (4 + n)H \longrightarrow MoNi_3 + 4OH^- + nH_{\text{included}} \quad (4)$$

Such a reaction is obviously an overall process whose elementary steps and their coupling with the slow surface reaction are not yet elucidated. No data are available on the species which undergo reduction. It might be the tetravalent Mo species (Ni_4MoO_2) rather than the hexavalent molybdate or a complex citrate/molybdate compound as for Cr discharge where a $(HCr_3O_{10}, nHSO_4)^{(n+1)-}$ compound would be reduced [13]. However even in the case of Cr electrocrystallization which can be separately deposited in strong acidic electrolytes, the role of the low valency state oxides is not well elucidated. The compounds MoO_2Ni_4 and $MoNi_3$ are written according to the analysis results. However they could not be identified by X-ray diffraction since the deposits were amorphous or poorly crystallized.

At higher polarization, due to the low bulk molybdate concentration, the diffusion of the molybdate species towards the cathode limits the molybdenum discharge. This can generate the capacitive feature observed in the plot in Fig. 3d, whose characteristic frequency is proportional to the electrode rotation speed and is independent of potential, as depicted in Fig. 6. The Ni/Mo ratio in the alloy deposit then increases, resulting in an improved crystalline state (larger grain size, lower microstress) as already mentioned (2b). The Ni–Mo solid solution could then be characterized in this range of potential where reaction (1) reassumes importance on the crystalline structure, somewhat similarly to hydrogen evolution on a nickel substrate.

Conclusions

Polarization and a.c. impedance measurements coupled to chemical and surface analysis have given some new insights into the molybdenum discharge mechanism. A reaction scheme is proposed based on the multi-step reduction of molybdate species. Three potential ranges may be distinguished according to the polarization and impedance data. At low polarization, a molybdenum oxide, possibly MoO_2, formed by molybdate reduction transforms, due to the presence of Ni^{2+} ions, into a mixed Ni–Mo oxide which catalyzes hydrogen evolution generated by citrate reduction. When the polarization is increased the mixed oxide is further reduced to a surface compound which inhibits hydrogen evolution. This slow reaction is coupled to the fact reaction leading to the Ni–Mo alloy deposit. At still higher polarization, due to the low molybdate concentration of the electrolyte, the molybdenum discharge is limited by diffusion, thus decreasing the molybdenum content in the deposited alloy.

References

[1] E. Chassaing and K. Vu Quang, *Electrodeposition and Surf. Treatment* **2** (1973/74) 65.
[2] K. Vu Quang, E. Chassaing, F. Bourelier and J. Montuelle, *Corrosion T.P.F.* **19** (1971) 237.
[3a] M. Cherkaoui, E. Chassaing and K. Vu Quang, *Plating and Surf. Finishing*, Oct. (1988) 50.
[3b] M. Cherkaoui, E. Chassaing and K. Vu Quang, *Advanced Materials and Manufacturing Processes* **3** (1988) 407.
[4] C. C. Nee, W. Kim and R. Weil, *J. Electrochem. Soc.* **135** (1988) 1100.
[5] A. Brenner in 'Electrodeposition of Alloys', Academic Press, New York and London (1963) Vol. 2, p.429.
[6a] H. Fukushima, T. Akiyama, S. Akagi and K. Higashi, *Trans. Japan Inst. Metals* **20** (1979) 358.
[6b] H. Fukushima, T. Akiyama and K. Higashi, *Kinzoku Hyomen Gijutsu* **32** (1981) 58.
[7] G. Charlot in "Les Méthodes de la Chimie Analytique Quantitative", Masson et Cie, Paris (1964) p. 807.
[8] E. Chassaing, M. Cornet and K. Vu Quang *Surf. Technology* **7** (1978) 14.
[9] F. A. Kroeger, *J. Electrochem. Soc.* **125** (1978) 2028.
[10] G. D. Wilcox, D. R. Gabe and M. E. Warwick, *Corrosion Sci.* **28** (1988) 577.
[11] 'Standard Potentials in Aqueous Solutions' (edited by A. J. Bard, R. Parsons and J. Jordon), M. Dekker Inc., New York (1985) p. 485.
[12] D. E. Brown, M. N. Mahmood, M. C. M. Man and A. K. Turner *Electrochim. Acta* **29** (1984) 1551.
[13] J. P. Hoare in 'Proc. Symp. Electrodeposition Technology, Theory and Practice' (edited by L. T. Romankiw), The Electrochem. Soc. Inc., **87** (1987) 233.